International Journal of Plasticity 169 (2023) 103710

Contents lists available at ScienceDirect

International Journal of Plasticity

journal homepage: www.elsevier.com/locate/ijplas

Beyond Orowan hardening: Mapping the four distinct mechanisms associated with dislocation-precipitate interaction

Shenyou Peng [a], Zhili Wang [a], Jia Li [a], Qihong Fang [a,*], Yujie Wei [b,c,**]

[a] College of Mechanical and Vehicle Engineering, Hunan University, Changsha 410082, China
[b] LNM, Institute of Mechanics, Chinese Academy of Sciences, Beijing 100190, China
[c] Eastern Institute for Advanced Study (EIAS), Ningbo 315200, China

ARTICLE INFO

Keywords:
Dislocation
Precipitate
Orowan hardening
Radiation-emission
Interface-nucleation

ABSTRACT

The conventional role played by precipitates in crystalline solids is in blocking the motion of dislocations and for consequentially hardening, a mechanism attributed to Orowan's finding. Recent experiments and theoretical analysis demonstrated that a few nanometre-sized precipitates, when dispersed in advanced metals at fine spacing, can further boost their strength at no sacrifice in ductility. In this paper, we construct the deformation map of four distinct mechanisms associated with dislocation-precipitate interaction: at low-to-intermediate stress level, dislocations may loop around a precipitate or cut-through it. In both scenarios the precipitates harden the materials and there is no net gaining of dislocations. At high stress level, nanoscale precipitates may in contrast act as dislocation sources and generate dislocations from the matrix-precipitate interface — an interface-nucleation process; or emit dislocations when highly stressed dislocations transverse them — a radiation-emission process. While the interface-nucleation mechanism could supply sustainable dislocation multiplication, the radiation-emission leads to the multiplication of two additional dislocations. Based on large-scale simulations and theoretical analysis, we construct a deformation map on dislocation-precipitate interaction in terms of stress and precipitate size. The revealed mechanisms and the dislocation-precipitate interaction map pave the way for strength–ductility optimization in materials through precipitation engineering.

1. Introduction

The vital mechanical properties of crystalline materials, such as strength and ductility, are closely related to the dislocation mobility and the interaction between dislocations with other microstructures (Anderson et al., 2017). The interaction between dislocations and precipitates is one of the most prominent mechanisms affecting the strength and toughness of metals. Traditionally, precipitates are thought to serve as obstacles to dislocations glide and harden the materials in hence (Argon, 2008; Ardell, 1985; Gladman, 1999). The well-known Orowan mechanism and cut-through mechanism are the basic strengthening origins in metals, and has been wildly applied in metallic alloying (Poole et al., 2005; Sjölander and Seifeddine, 2010; Proville and Bakó, 2010; Singh and Warner, 2010; Wu et al., 2020; Krasnikov et al., 2020; Fomin et al., 2021). Nevertheless, the accumulation of dislocations in front of

* Corresponding author.
** Corresponding author at: LNM, Institute of Mechanics, Chinese Academy of Sciences, Beijing 100190, China.
E-mail addresses: fangqh1327@hun.edu.cn (Q. Fang), yujie_wei@lnm.imech.ac.cn (Y. Wei).

https://doi.org/10.1016/j.ijplas.2023.103710
Received 17 May 2023; Received in revised form 8 July 2023; Accepted 19 July 2023
Available online 22 July 2023

obstacles can lead to stress concentration, resulting in reduced ductility of engineering materials (Weertman and Keer, 1997; Lu, 2010; Ritchie, 2011; Shao et al., 2018). Therefore, the Orowan mechanism is not preferred over other strengthening methods when mitigating strength-ductility trade-off in crystalline metals is concerned (Ritchie, 2011; Sun et al., 2020).

Recent years, numerous studies have shown that it is possible to enhance not only the strength but also the ductility of materials simultaneously by designing the nanoprecipitates properly (Shi et al., 2015; Raabe et al., 2009; Kim et al., 2015; He et al., 2016; Jiang et al., 2017; Li et al., 2017; Ming et al., 2018; Sun et al., 2018; Yang et al., 2018; Lei et al., 2018; Jiang et al., 2022). The underlying interactions between dislocations and nanoprecipitates is then ought to be crucial. In present, a large number of papers have been devoted to atomistic modeling of the interaction of dislocations and the nanometer inclusions (Xiong et al., 2015; Krasnikov and Mayer, 2019; Singh and Warner, 2010; Esteban-Manzanares et al., 2019). For nanoscale precipitates, the crystallographic coherence with surrounding matrix is a critical factor affecting the strength and ductility optimization (Lu et al., 2009). However, experiments and simulations have shown a more complex interaction mechanism between dislocation and precipitates, especially at the nanoscale (Ashby and Johnson, 1969; Tan and Tice, 1976; Peng et al., 2020; Yang et al., 2021; Bao et al., 2022). Peng et al. (2020) revealed that nanoprecipitates provide a sustainable dislocation source. A dense dispersion of nanoprecipitates served as both dislocation sources and obstacles, leading to a virtuous cycle between ductility and strength. Further modeling (Yang et al., 2021; Bao et al., 2022) in Cu alloys confirmed that nanoprecipitates can not only hinder dislocation movement, but also promote dislocations multiplication. It is noted that most theoretical and numerical studies on the interaction between dislocation and precipitation focused on quasi-static state (Ardell, 1985; Singh and Warner, 2010; Fan et al., 2018; Fang et al., 2019; Szajewski et al., 2020). High-speed dislocations resulted from high stress and their dynamic effect are rarely mentioned. Indeed, stressed dislocations could be supersonic (Gumbsch and Gao, 1999; Tsuzuki et al., 2009; Peng et al., 2019). Therefore, the interaction between high-speed dislocations and nanoscale precipitates are essential for the understanding the hardening mechanism in high strength metals. More importantly, mechanisms associated with dislocation-precipitate interaction are often documented separately. A comprehensive understanding regarding the dominance of individual mechanisms at specific stress levels and for precipitates of different size is lacking. Such a deformation map, if physically faithful, would pave the way for precipitate engineering in high strength metals.

2. Methods and results

Atomistic simulations were performed to investigate the interaction between high-speed dislocations and nanoscale precipitates in face centered cubic (FCC) nickel. Since a full dislocation in FCC crystal glides on the [111] planes and along the ⟨110⟩ directions, the x, y, z coordinates of the simulation box are set to be parallel to the $[\bar{1}\bar{1}2,\ 111,\ 1\bar{1}0]$ crystallographic directions, respectively, as shown in Fig. 1a. An edge dislocation was realized by removing a column of atoms with a net thickness equal to the Burgers vector. After relaxation, a complete dislocation resolves into two Shockley partial dislocations, here the dislocation line represents the full

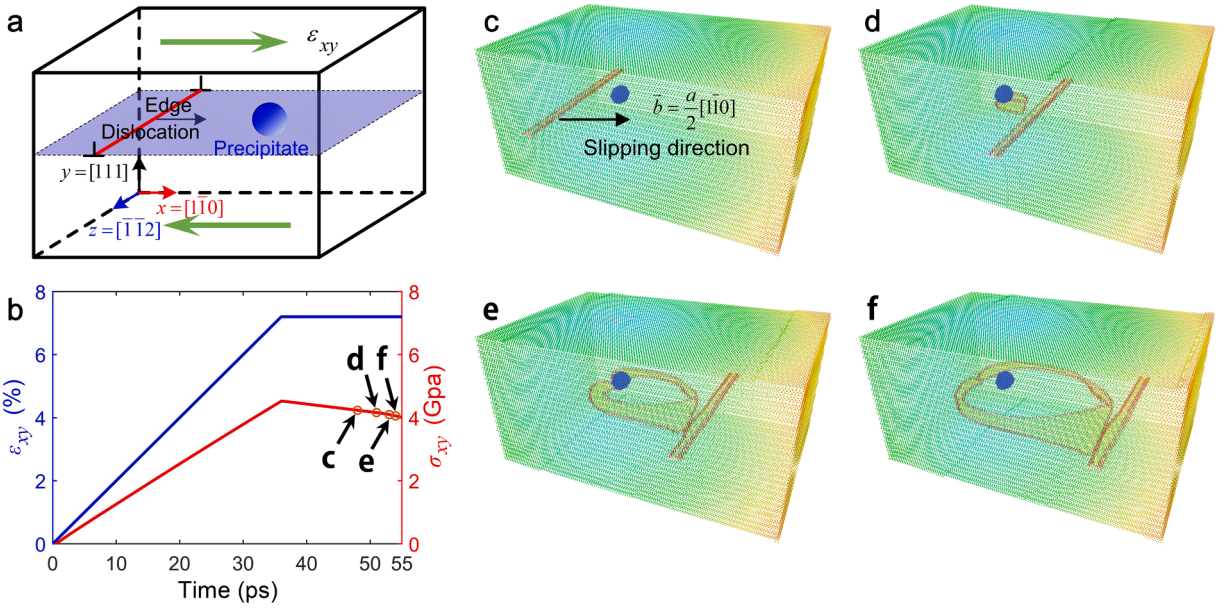

Fig. 1. Interaction between a high-speed dislocation and a nano-precipitate. (a) The initial setup in the periodic sample with an edge dislocation (the red line) and a nano-precipitate (Cr in blue), which is embedded in FCC Ni and near to the slip plane (in blue) of the dislocation. The crystallographic orientation is set to be $\boldsymbol{x} = [\bar{1}\bar{1}2], \boldsymbol{y} = [111], z = [1\bar{1}0]$ in the matrix; Shear strain $\boldsymbol{\varepsilon_{xy}}$ is apllied to accelerate the dislocation. (b) The shear stress ($\boldsymbol{\sigma_{xy}}$) and strain ($\boldsymbol{\varepsilon_{xy}}$) vs. time. Before interacting with precipitates, the dislocation moves at a constant speed. (c)-(f) The atomic structure snapshots corresponding to the stress state keyed in (b). Here Ni atoms are colored to highlight the structure of emitted dislocations, with Cr precipitate atoms in blue.

dislocation for simplicity. In addition, we constructed the spherical nano-precipitate by replacing a number of Ni atoms with coherence Cr and preserving the FCC structure. The size of nano-precipitates is about 2–5 nm, which is small enough to maintain a coherent interface between the matrix and the precipitate. The precipitate is located in front of the edge dislocation, and the two will interact with each other after a strain load ε_{xy} to accelerate the dislocation. All simulations were performed in the large-scale atomic/molecular massively parallel simulator (LAMMPS) (Plimpton, 1995). The embedded atom method (EAM) potentials (Howells and Mishin, 2018) were adopted here to capture the atomic interactions between Cr-Cr, Cr-Ni, and Ni-Ni atoms. The size of all periodic simulation boxes is about 161.8 × 30.3 × 21.4 nm, containing 9.74 million atoms. Featured atoms were traced by common neighbor analysis (CNA) and dislocation extraction algorithm (DXA) in OVITO (Stukowski, 2010).

After energy minimization and structure relaxation at an initial temperature of $T = 1$K, we apply shear strain ε_{xy} at a constant strain rate of 2×10^8 s^{-1} under the microcanonical NVE ensemble until the dislocation reaches a high speed, then we keep the strain constant to ensure the dislocation interact with precipitate at given stress. Fig. 1b illustrated the stress-time and strain-time curves resulting from the loading strategy. In our simulation, the final elastic strain is about $\varepsilon_{xy} = 7.2\%$ and the dislocation moves at a steady

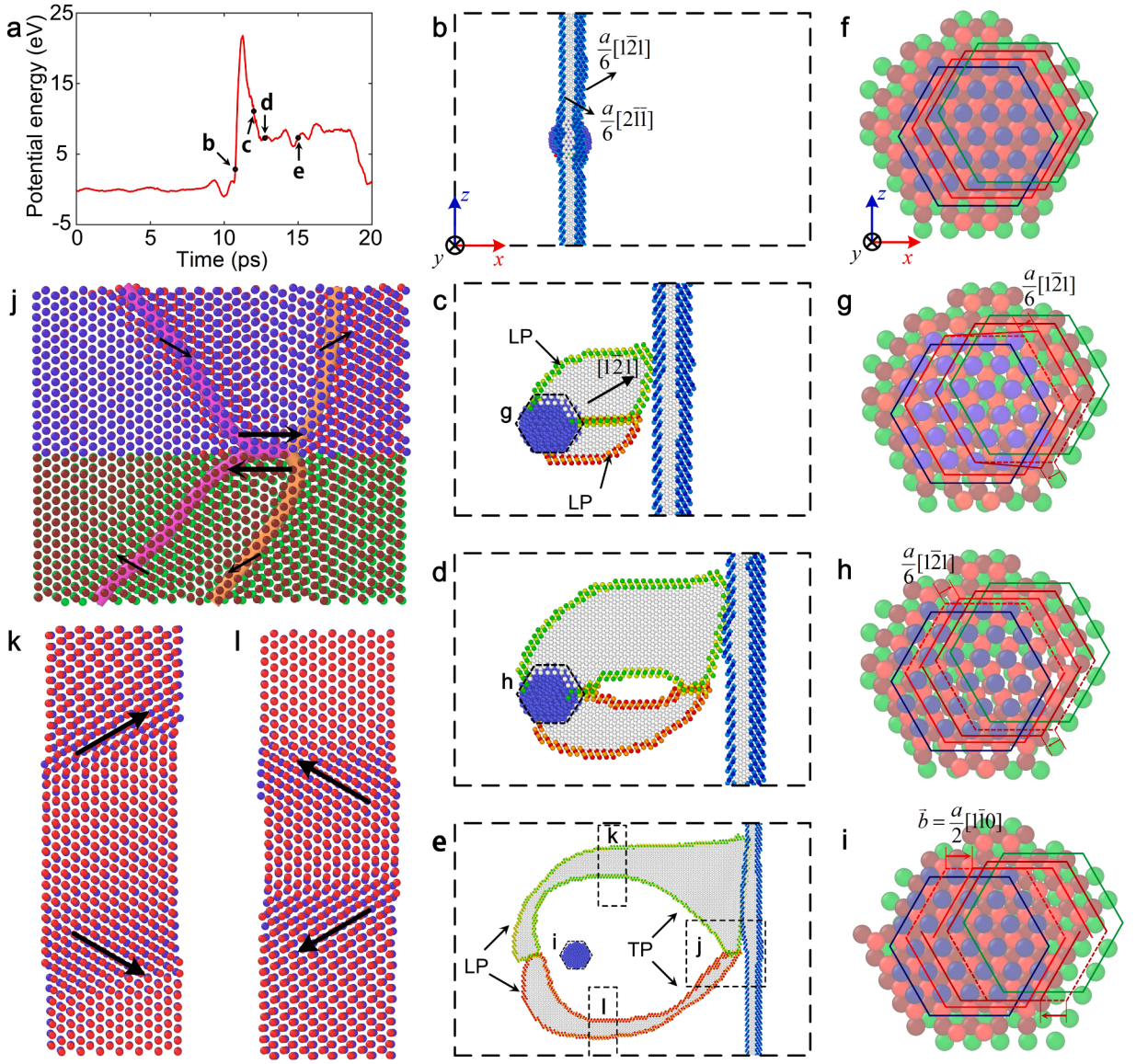

Fig. 2. Atomic resolution to show the radiation-emission during high-speed dislocation-precipitate interaction. (a) The evolution of the total potential energy of the precipitate (normalized by that of its intial static state). (b)-(e) Detailed atomic structure corresponding to the state marked in (a). Atoms are colored by their y-coordinates and only the dislocation and the precipitate are illustrated. (f)-(i) Detailed atomic evolution of the precipitate corresponding to (b)-(e). The colored hexagons represent the close-packed configuration of different layers, with dashed lines for the initial position, and solid lines for the displaced position. (j)-(l) Detailed atomic structure of the two emitted dislocations. The opposite direction of LP pairs and TP pairs, shown in black arrows, ensures the conservation of the Burgers vector.

speed of $v = 3.4\text{km/s}$ before interacting with the spherical nano-precipitate of radius $r = 1.09\text{nm}$. After the dislocation collides with the precipitate, the dislocation continues to move on its original gliding plane with a slight velocity drop due to the barrier effect, and dislocation loops nucleated from the precipitate afterwards. Corresponding atomic structures are shown in Fig. 1c-f. Affected by the high-speed dislocation, a pair of dislocations were generated from the junction of the nano-precipitate and the matrix, and propagate in two symmetric directions on the [111] plane. The nucleated dislocation pair also move at high speeds. The whole process of the interaction between high-speed dislocation and nanoprecipitates shows a novel mechanism differing from the traditional Orowan mechanism and the cut-through mechanism, and it provides a new dislocation origin at high stress levels. Complementary dynamics to show the interacting process can be seen in Movie 1 and Movie 2.

As the high-speed dislocation move through the precipitates, atoms in its proximity are disturbed. The potential energy of the precipitate atoms is shown in Fig. 2a, and the corresponding atomic structural evolutions are shown in Fig. 2b-e. Here we presented a planar view with the dislocation lines coloured by y-coordinates. Once the dislocation interacts with the precipitates (shown in Fig. 2b), the potential energy increases rapidly as the high-speed dislocation brings kinetic energy and introduces atomic distortion. A pair of leading partial (LP) dislocations are nucleated from the nano-precipitate in order to lower the energy, as shown in Fig. 2c. It is worth noting that the LP dislocations are nucleated from different layers, and its Burgers vector is in the opposite direction to maintain the coherency between precipitate and the matrix, which are marked by the arrows shown in Fig. 2k-l. As the leading partials run away, the stacking fault between the leading partials and the trailing partials (TP) stretches — a region shown in gray, resulting in rapidly expanding of the stacking-fault area. As a consequence, the TPs are nucleated afterward and, in combination with the LPs, form two pairs of full dislocations, see Fig. 2d-e. In Fig. 2f-I, we show how adjacent atomic layers in the precipitate shift with respect to the snapshots shown in Fig. 2b-e, in turn. During the interaction, two partials are firstly nucleated from two neighboring layers in the precipitate, as shown in Fig. 2f-h. The colored hexagons shows the atomic configuration in two adjacent close-packed planes. the atomic displacement is exactly one Burgers vector $\frac{a}{6}[1\bar{2}1]$ of a partial dislocation, as illustrated in Fig. 2g-h. Afterward, the full dislocation pairs are formed, with atomic displacement shown in Fig. 2i. The radiation-emission process leaves a sheared precipitate by one Burgers vector and two emitted dislocations. It is noted that, as the dislocations emitted in different layers from the precipitates, the junctions between the nucleated dislocation pairs are always joined together to maintain atomic coherence, as shown in Fig. 2j, which is circled in Fig. 2e.

As a comparison, the interaction between dislocations and precipitates in two-dimensional (2D) samples is investigated also. The size of periodic 2D simulation boxes is about $373.6 \times 182.9 \times 0.8$ nm containing 5.4 million atoms. The precipitate is located on the slip plane of the edge dislocation as shown in Fig. 3a. The coordinates are defined by the crystallographic orientations $x = [1\bar{1}0], y = [111], z = [\bar{1}\bar{1}2]$. The same loading strategy as the three-dimensional samples is employed, and its corresponding stress-time and strain-

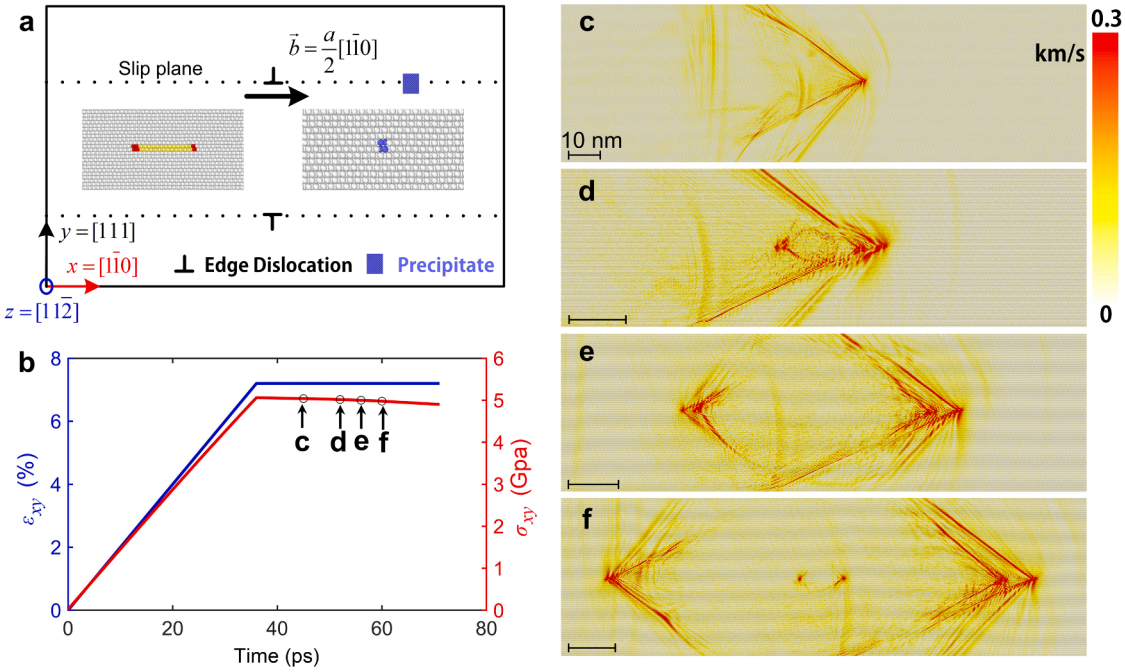

Fig. 3. Interaction between the high-speed dislocation and the nano-precipitate in two dimensional samples. (a) The two-dimensional simulation sample with edge dislocation and nano-precipitate. Dislocation dipoles are created to maintain a zero-sum Burgers vector. The relaxed atomic structure is shown on the left. The precipitate of Cr is embedded in a perfect FCC matrix of Ni, with atomic structure shown on the right. (b) The shear stress (σ_{xy}) / applied strain (ε_{xy}) - time curves. Before interacting with precipitates, the dislocation moves at a high speed steadily with the sample remains elastic. (c)-(f) Detailed dislocation dynamics during the interaction process corresponding to the state marked in (b). The color of the atoms represents the velocity of the atoms.

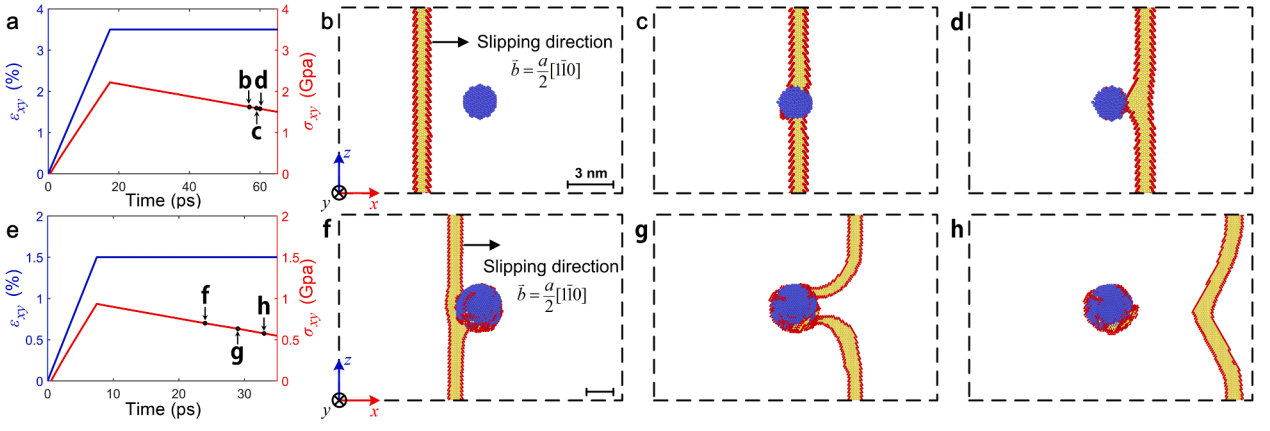

Fig. 4. Shearing and Orowan mechanism between dislocation-precipitate interaction. (a)-(d) The shear stress ($\boldsymbol{\sigma}_{xy}$) and applied strain ($\boldsymbol{\varepsilon}_{xy}$) vs. time curves and atomic structural evolution during the cut-through process. (e)-(h) The shear stress ($\boldsymbol{\sigma}_{xy}$) and strain ($\boldsymbol{\varepsilon}_{xy}$) vs. time curves and atomic structural evolution during Orowan interaction. Atoms are colored based on their common neighbor analysis (CNA) values to show the dislocation structure.

time curves are shown in Fig. 3b. The radiation-emission mechanism is observed more clearly. As a typical result, the atomic velocity field shows the detailed dislocation dynamics in Fig. 3c-f. Before the interaction, the high-speed dislocation induces a propagating stress field and atomic velocity field shown in Fig. 3c, with the elastic strain is about $\varepsilon_{xy} = 7.2\%$ and the dislocation speed is about 4.83km/s. After the dislocation collides with the nano-precipitate, the dislocation continues to move on its gliding plane with a slight velocity drop due to the barrier effect by precipitates, and two pairs of dislocations nucleated from the precipitate afterwards (shown in Fig. 3d-f). The complementary interacting process of 2D samples can be seen in Movie 3.

This newly observed radiation-emission is an efficient dislocation nucleation mechanism, rather than typical obstacle effect on dislocation activities in existing observations. We suspect that typical in-situ experiments using transmission electron microscope may not be able to capture the kinetics of those fast-moving dislocations. The usage with in-situ high-energy particles for dynamic behavior of metals may make it possible in identifying those distinct dislocation mechanisms.

3. Discussion

High-speed dislocation promotes dislocation emission from nano-precipitates, this novel mechanism differs from the traditional Orowan or cut-through interaction between dislocation and precipitates. According to Peng et al. (2020), coherent nano-precipitates nucleate dislocation at the interface under high stress levels — the interface-nucleation mechanism. We suppose the high-speed moving dislocation, which carries kinetic energy and lattice distortion, provides the additional energy for dislocation emission.

Same as the hardening mechanism of nano-precipitates on materials, the nucleation mechanism of nano-precipitates is closely related to the nano-precipitation size and applied stress. In order to explore the conditions for nano-precipitate nucleating dislocation when interacting with high-speed dislocation, and to broaden the understanding of the various mechanisms of dislocations and nano-precipitate inside metallic materials, we simulated samples with initial edge dislocations and nano-precipitates of different sizes and subjected to different stress levels.

As shown in Fig. 4, the cut-through (shearing) mechanism and Orowan mechanism between the dislocation and the nano-precipitate were also observed in our simulation at specific stress state and precipitation size. At high stress levels with small precipitates, the interaction between edge dislocation and precipitates shows a cut-through behavior (Fig. 4a-d). The dislocation cuts the precipitate, and its gliding speed and shape are nearly unchanged. As a comparison, we show in Fig. 4e-h the Orowan mechanism in a sample with larger precipitates and subjected to lower stress, the dislocation is pinned by the precipitates and bowing out, when the bowing angle reaches a critical value, the dislocation flees from the pinning sites, left a residual dislocation line surrounding the precipitates.

Taking into account the interface-nucleation mechanism (Peng et al., 2020), four types of interacting mechanisms between dislocation and nano-precipitates are concluded. (1) Cut-through mechanism, the nano-precipitates are sheared by the gliding dislocation, and act as “soft” particles. (2) Orowan mechanism, dislocation bypasses the precipitate leaving a dislocation ring around the precipitate, acting as “hard” particles (Gladman, 1999). (3) Interface-nucleation mechanism, nano-precipitates nucleate dislocations at high stress level without interacting with gliding dislocations (Peng et al., 2020). (4) Radiation-emission mechanism, dislocation emitted when the precipitate interacts with a high-speed dislocation. The animations of those four mechanisms are shown in the Movie 1 and Movie 2.

We further performed a series of simulation to construct the deformation map between dislocation-precipitate interaction with different precipitation sizes and external stresses. While the speed of dislocation is a direct factor that determines the interaction mechanism, we adopt stress a controlling variable for convenience, which could be readily abstracted from a stress-strain curve. The

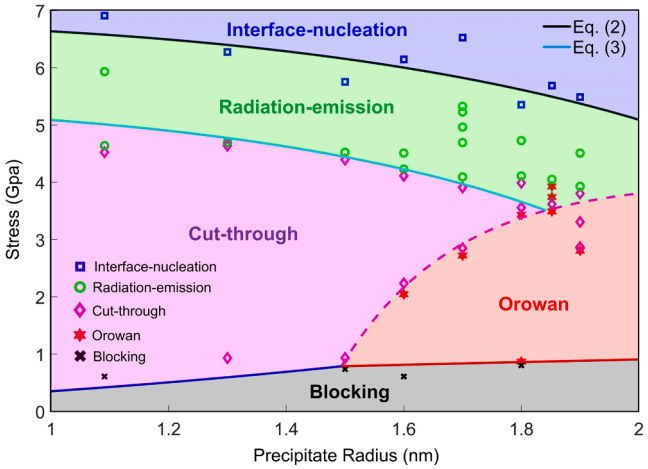

Fig. 5. The deformation map of dislocation-precipitate interaction for different precipitation sizes and stresses. Symbols come from simulations, and domains of different colours reflect distinct deformation mechanisms. The four regions for four interaction mechanisms are separated by the boundaries detailed in the text. The bottom region in gray showing dislocations to be blocked by precipitates at low stress level.

velocity is not straightforward as the relationship between stress and dislocation velocity is nonlinear at high stress levels. As shown in Fig. 5, four types of interaction are presented in different colored regions, the data points represent our typical simulation results and distinguished the critical boundaries. For coherent nano-precipitates, cut-through mechanism and Orowan mechanism happen at low stress levels with small precipitate for shearing and large particle for Orowan, those mechanisms harden the materials as the precipitates act as obstacle to dislocation gliding. On the contrary, interface-nucleation and radiation-emission occur at high stress levels with large precipitate for interface-nucleation and small particle for radiation-emission, and both mechanisms enhance the ductility of materials as the precipitates promote nucleation of dislocations. The competitive mechanisms activated at different nano-precipitation sizes and applied stresses determine the mechanical behavior of crystal materials. We illustrate how the boundaries may be determined based on energetic criteria in the following.

Based on the energy analysis of Peng et al. (2020), we proposed that the energy criterion for dislocation emission in the form of

$$E_{str} + E_{pre} + E_{dis} = E_c \tag{1}$$

where $E_{str} = \sigma^2 V_0 / G$ represents the deformation energy under the applied shear stress loading σ, V_0 the activation volume for dislocation nucleation, ranging from $10b^3$ to $10^4 b^3$ according to different dislocation mechanisms (Conrad, 1964), and $G = 72$GPa is the shear modulus of Ni matrix. E_{pre} denotes the distortion energy of the precipitate. Using Eshelby's solution for an ellipsoidal dilatation inclusion (Eshelby and Peierls, 1957), the distortion energy E_{pre} of a misfit precipitate follows $E_{pre} \propto G\left(\frac{a_p - a_m}{a_m}\right)^2 r^3$, with a_p and a_m are the lattice constants of the precipitate and the matrix, and r is the radius of the precipitate. E_{dis} denotes the total energy of the moving dislocation, here we ignored its detailed components such as static energy, dynamic energy and dissipative energy caused by lattice friction (Kim et al., 2020). The term E_c denotes the critical energy for dislocation nucleation, i.e. dislocation emission occurs when the energy reaches a critical value E_c. Simiar to the form of E_{str}, one may also connect the critical energy to critical stress by $E_c = \sigma_c^2 V_0 / G$.

For the interface-nucleation case, $E_{dis} = 0$, we obtain

$$\sigma_{i-n}^2 = \sigma_c^2 - \beta G^2 \left(\frac{r}{b}\right)^3 \tag{2}$$

where β is a nondimensional parameter associated with the distortion between matrix and precipitates. We show in Fig. 5 that theory prediction of Eq. (2) agrees well with our simulation results by using $\beta = 7.7 \times 10^{-6}$, $\sigma_c = 6.8$GPa.

Our simulations show that, to trigger radiation-emission, high stresses are required. Consequentially, dislocations moving at high-speed as a resultant of high external stress radiates energy through front waves. We may consider E_{dis} a constant since the speed of the dislocation become a constant at high stress (Gumbsch and Gao, 1999; Tsuzuki et al., 2009; Peng et al., 2019). Therefore, the radiation-emission curve in Fig. 5 becomes

$$\sigma_{r-e}^2 = \sigma_c^2 - \beta G^2 \left(\frac{r}{b}\right)^3 - \frac{G E_{dis}}{V_0} \tag{3}$$

with $\frac{G E_{dis}}{V_0} = 18.2\ (\text{GPa})^2$.

It is worth noting that the dislocation nucleation occurs when a precipitate is subject to the stress wave from a high-speed dislocation. That is, the stress wave can facilitate the emission in the absence of direct contact between the dislocation and the precipitation. These results indicate that the dynamic energy of the moving dislocation is the dominate factor responsible for radiation-emission.

The equations agree well with our simulation results for precipitates at nano scale (about 2 to 5 nm). For larger size of precipitation, the interaction mechanism will be mostly characterized by interfaces due to its incoherent interfacial structure. In such scenarios (Bao et al., 2022), the trend should remain consistent with Fig. 5 as the interfacial dislocations may be readily available. On the other side, inhomogeneous stress fluctuations may occur inside the material at micro to nanoscale even under uniform external loads due to lattice defects, such as grain boundary (Capolungo et al., 2007; Benkassem et al., 2007) or crack tip (Cemal Eringen and Kim, 1974), leading to localized ultra-high stresses. The presented dislocation multiplication at high-stress provides a novel mechanism to reduce stress concentration

The Orowan and cut-through hardening effect are also illustrated in Fig. 5. Those simulations are well agreed with the hardening theory (Proville and Bakó, 2010). When $r < 1.5$nm, the interaction is cut-through in nature, with a threshold stress $\sigma_{cut} = \frac{\sigma_m \pi r}{L d_{spd}}$, with $\sigma_m = 4.6$GPa being the critical stress, $L = 22$nm is the inter-precipitate distance, and $d_{spd} = 1.9$nm is the dislocation dissociation width. The relation is shown in blue solid line. When $r > 1.5$nm, the Orowan looping activated; the critical stress to overcome precipitate blocking is estimated to be $\sigma_{Orowan} = \frac{2-\upsilon}{4(1-\upsilon)} \frac{Gb}{2L - \pi r} \left[\ln\left(\frac{4r}{\rho}\right) - 2\right]$. For the Poisson's ratio $\upsilon = 0.28$ and $\rho = 0.05$nm, we obtain the red solid line shown in Fig. 5.

According to Fig. 5, greater precipitates enhance the strengthening effect due to cut-through and Orowan mechanisms and soften the materials by Interface-nucleation and Radiation-emission mechanisms. The competition between those mechanisms determines the strength and/or ductility in materials. Therefore, the optimal precipitate size that enhances the yield stress without the loss of ductility will be found when the strengthening effect is on par with the softening part (Peng et al., 2020; Bao et al., 2022). It provides a foundation for strength–ductility optimization in materials designing.

It is noted that, traditionally, the shift between cut-through mechanism and Orowan mechanism only depends on the particle size (Ardell, 1985; Poole et al., 2005; Fomin et al., 2021). In fact, the conversion between the two mechanisms is complicated. C. Singh and D. Warner (Singh and Warner, 2010) have studied the interactions of edge dislocations with Guinier–Preston zones in Al–Cu alloys and

identified a new mechanism that the leading partial cuts the GP zone and the trailing partial loops around it. Krasnikov and Mayer (Krasnikov et al., 2020) have studied the interaction of edge dislocations with the θ' phase, Orowan mechanism was observed with low shear stress and θ' phase was cut by dislocation with high shear stress. In this work, we see that the stress also becomes an important factor affecting the transition between cut-through and Orowan mechanisms in Fig. 5. We show the Orowan and cut-through mechanisms under different stresses with constant precipitation size $r = 1.8$nm in Fig. 6. Under lower external stress, $\sigma = 1.08$GPa for instance, the dislocation bows around the nano-precipitate, leaving a dislocation ring surrounding the nano-precipitate. A misfit of 0.139 nm $\approx b/2$ remains in the nano-precipitate. Nevertheless, when the external stress is high, $\sigma = 3.62$GPa in this case, the interaction changes to cut-through type, as shown in Fig. 6d-f. The dislocation shears the nano-precipitates undeformed, leaving a misfit of 0.253 nm $\approx b$. This transitional phenomenon between cut-through mechanism and Orowan mechanism under different external stresses enriches the interaction mechanism between dislocations and precipitates.

Four similar dislocation-precipitate interaction are also found in 2D simulations. Noting that the Orowan mechanism happens in 3D samples only, we name Orowan-like mechanism to clarify a new mechanism in 2D simulations. In this mechanism, dislocation change the precipitate configuration when passing through the precipitates, differ from the cutting through mechanism, which will not change the precipitate configuration after passing the precipitates. The interface-nucleation and radiation-emission mechanism shows the similar phenomenon as 3D simulations. The dynamics of the four mechanisms are shown in Movie 4.

Four types of interaction mechanism are included and shown in different colored regions based on a series of simulation with different precipitation sizes and external stresses, as shown in Fig. 7. The data points represent our simulation results and distinguished the critical boundaries of the four distinct mechanisms. Same as the 3D results, cut-through and Orowan-like mechanisms happen at low stress levels with small precipitate, those mechanisms harden the materials as the precipitates act as obstacle to dislocation gliding. On the contrary, interface-nucleation and radiation-emission mechanisms happen at high stress levels with large precipitate, those mechanisms enhance the ductility of materials as the precipitates promote the nucleation of dislocations.

Similar to the 3D cases, the energy equilibrium equation of interface-nucleation mechanism in 2D simulation should be expressed as

$$\sigma_{i-n}^2 = \sigma_c^2 - \beta G^2 \left(\frac{r}{b}\right)^2 \tag{4}$$

with the Eshelby's inclusion energy of a misfit precipitate fallows $E_{pre} \propto G\left(\frac{a_p - a_m}{a_m}\right)^2 r^2$ in 2D cases. The theory prediction agrees well with the simulation results using $\beta = 8.4 \times 10^{-3}$ and $\sigma_c = 5.64$GPa. For radiation-emission mechanism, $E_{dis} > 0$, the dislocation nucleation become easier. As the speed of moving dislocation, thus the E_{dis}, and applied stress are nonlinearly related (Tsuzuki et al., 2009). The explicit equilibrium equation is hard to conclude, but the trend is clear. At low stress, the moving dislocation moving at a low speed and the energy can hardly radiate from dislocation core, the dislocation nucleation mechanism is not activated. At high stress levels, especially above 2.5 GPa in our simulation, the high-speed dislocation radiates the concentrated energy and stress from dislocation

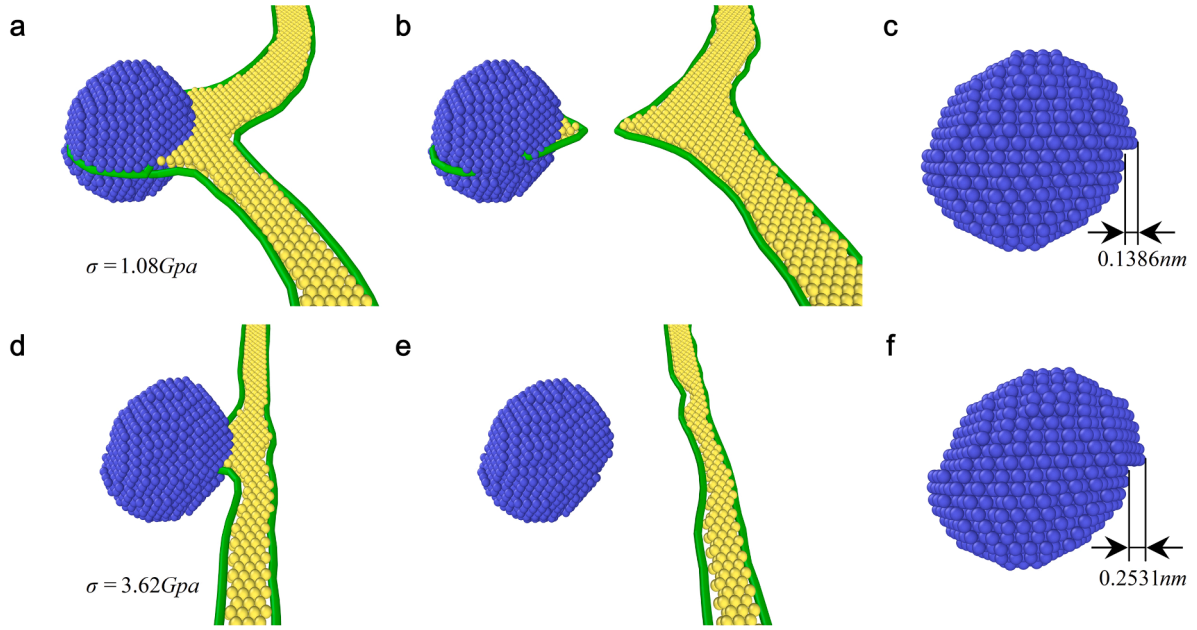

Fig. 6. The transition between Orowan looping and shearing at different external stresses with precipitation size $\boldsymbol{r} = 1.8$ **nm**. (a)-(c) The Orowan looping at stress $\boldsymbol{\sigma} = 1.08$**GPa**. (a) and (b), the looping process, (c) the deformed nanoprecipitate with a misfit of 0.139 **nm** $\approx \boldsymbol{b}/2$. (d) and (e) The cut-through mechanism at stress $\boldsymbol{\sigma} = 3.62$**GPa**, (f) the deformed nanoprecipitate with a misfit of 0.253**nm**, which is about one Burgers vector.

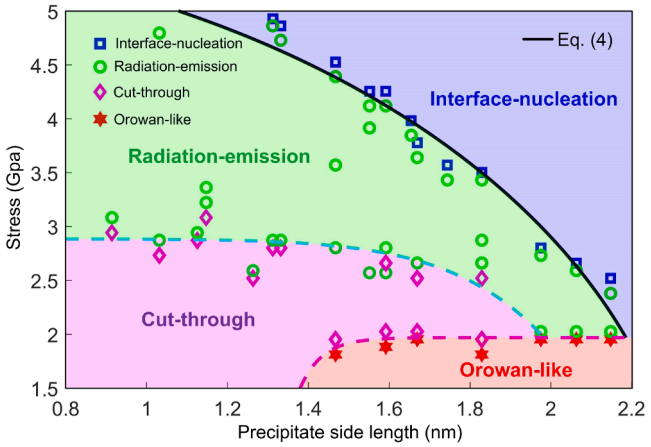

Fig. 7. The interaction map between dislocation and precipitate with different precipitation sizes and external stresses in two-dimensional simulations. The abscissa represents the side length of the square shaped precipitates. The simulation results are demonstrated as points in different shapes and colours. The four regions, denoting four interaction mechanisms, are divided by the fitted boundaries.

core, and the dislocation nucleation becomes the dominate mechanism.

4. Conclusion

In summary, we explored the dislocation nucleation caused by the interaction between high-speed dislocation and nanoscale precipitates using large-scale MD simulations. It is revealed that a high-speed dislocation encountering a nanoscale precipitate promotes dislocation nucleation. This unique interaction between dislocations and precipitates, which differs fundamentally from the traditional Orowan or cut-through interaction mechanism, provides extra dislocation sources for enhanced ductility of high strength materials, complements the widely upheld perception that precipitates act as obstacles to dislocation motion.

Through large-scale simulations on dislocation-precipitate interactions in samples containing different size of precipitates and subjected to low-to-high stress levels both in 3D samples and 2D samples, we construct a deformation map associated with dislocation-precipitate interaction:Cut-through mechanism, Orowan mechanism, Interface-nucleation mechanism, and Radiation-emission mechanism. The interaction map shows the competition between obstacle effect and nucleation effect of nano-precipitates when interacting with moving dislocations. The nano-scaled precipitates tend to exhibit hardening mechanism at low stresses and toughening mechanism at high stresses. The Interface-nucleation mechanism and radiation-emission mechanism, which occurs at high stress level, can also promote the dislocation multiplication beyond Orowan hardening. Those findings may help establish a foundation for strength–ductility optimization through microstructure manipulation in high strength alloys.

CRediT authorship contribution statement

Shenyou Peng: Conceptualization, Methodology, Formal analysis, Writing – original draft. **Zhili Wang:** Methodology, Investigation, Formal analysis. **Jia Li:** Formal analysis. **Qihong Fang:** Formal analysis, Supervision. **Yujie Wei:** Conceptualization, Formal analysis, Writing – review & editing, Supervision.

Declaration of Competing Interest

The authors declare that they have no known competing financial interests or personal relationships that could have appeared to influence the work reported in this paper.

Data availability

Data will be made available on request.

Acknowledgments

The authors would like to deeply appreciate the supports from National Natural Science Foundation of China (12102133, 12172123, 12072109, and 11988102).

The simulations were conducted at the Supercomputing Center of CAS.

Supplementary materials

Supplementary material associated with this article can be found, in the online version, at doi:10.1016/j.ijplas.2023.103710.

References

Anderson, P.M., Hirth, J.P., Lothe, J., 2017. Theory of Dislocations, 3rd ed. Cambridge University Press, Cambridge.
Ardell, A.J., 1985. Precipitation hardening. Metall. Trans. A 16 (12), 2131–2165.
Argon, A.S., 2008. Strengthening Mechanisms in Crystal Plasticity. Oxford University Press, Oxford; New York.
Ashby, M.F., Johnson, L., 1969. On the generation of dislocations at misfitting particles in a ductile matrix. Philos. Mag. A J. Theor. Exp. Appl. Phys. 20 (167), 1009–1022.
Bao, H., Xu, H., Li, Y., Bai, H., Ma, F., 2022. The interaction mechanisms between dislocations and nano-precipitates in CuFe alloys: a molecular dynamic simulation. Int. J. Plast. 155, 103317.
Benkassem, S., Capolungo, L., Cherkaoui, M., 2007. Mechanical properties and multi-scale modeling of nanocrystalline materials. Acta Mater. 55 (10), 3563–3572.
Capolungo, L., Spearot, D.E., Cherkaoui, M., McDowell, D.L., Qu, J., Jacob, K.I., 2007. Dislocation nucleation from bicrystal interfaces and grain boundary ledges: relationship to nanocrystalline deformation. J. Mech. Phys. Solids 55 (11), 2300–2327.
Cemal Eringen, A., Kim, B.S., 1974. Stress concentration at the tip of crack. Mech. Res. Commun. 1 (4), 233–237.
Conrad, H., 1964. Thermally activated deformation of metals. JOM 16 (7), 582–588.
Eshelby, J.D., Peierls, R.E., 1957. The determination of the elastic field of an ellipsoidal inclusion, and related problems. Proc. R. Soc. Lond. Ser. A. Math. Phys. Sci. 241 (1226), 376–396.
Esteban-Manzanares, G., Martinez, E., Segurado, J., Capolungo, L., LLorca, J., 2019. An atomistic investigation of the interaction of dislocations with Guinier-Preston zones in Al-Cu alloys. Acta Mater. 162, 189–201.
Fan, H., Ngan, A.H.W., Gan, K., El-Awady, J.A., 2018. Origin of double-peak precipitation hardening in metallic alloys. Int. J. Plast. 111, 152–167.
Fang, Q., Li, L., Li, J., Wu, H., Huang, Z., Liu, B., Liu, Y., Liaw, P.K., 2019. A statistical theory of probability-dependent precipitation strengthening in metals and alloys. J. Mech. Phys. Solids 122, 177–189.
Fomin, E.V., Mayer, A.E., Krasnikov, V.S., 2021. Prediction of shear strength of cluster-strengthened aluminum with multi-scale approach describing transition from cutting to bypass of precipitates by dislocations. Int. J. Plast. 146, 103095.
Gladman, T., 1999. Precipitation hardening in metals. Mater. Sci. Technol. Ser. 15 (1), 30–36.
Gumbsch, P., Gao, H., 1999. Dislocations faster than the speed of sound. Science 283 (5404), 965–968.
He, J.Y., Wang, H., Huang, H.L., Xu, X.D., Chen, M.W., Wu, Y., Liu, X.J., Nieh, T.G., An, K., Lu, Z.P., 2016. A precipitation-hardened high-entropy alloy with outstanding tensile properties. Acta Mater. 102, 187–196.
Howells, C.A., Mishin, Y., 2018. Angular-dependent interatomic potential for the binary Ni–Cr system. Modell. Simul. Mater. Sci. Eng. 26 (8), 085008.
Jiang, S., Wang, H., Wu, Y., Liu, X., Chen, H., Yao, M., Gault, B., Ponge, D., Raabe, D., Hirata, A., 2017. Ultrastrong steel via minimal lattice misfit and high-density nanoprecipitation. Nature 544 (7651), 460–464.
Jiang, M., Han, Y., Chen, X., Zu, G., Zhu, W., Ran, X., 2022. Cu-rich nanoprecipitates modified using Al to simultaneously enhance the strength and ductility of ferritic stainless steel. J. Mater. Sci. Technol. 121, 93–98.
Kim, S.H., Kim, H., Kim, N.J., 2015. Brittle intermetallic compound makes ultrastrong low-density steel with large ductility. Nature 518 (7537), 77–79.
Kim, S., Kim, H., Kang, K., Kim, S.Y., 2020. Relativistic effect inducing drag on fast-moving dislocation in discrete system. Int. J. Plast. 126, 102629.
Krasnikov, V.S., Mayer, A.E., 2019. Dislocation dynamics in aluminum containing theta ’ phase: atomistic simulation and continuum modeling. Int. J. Plast. 119, 21–42.
Krasnikov, V.S., Mayer, A.E., Pogorelko, V.V., 2020a. Prediction of the shear strength of aluminum with θ phase inclusions based on precipitate statistics, dislocation and molecular dynamics. Int. J. Plast. 128, 102672.
Krasnikov, V.S., Mayer, A.E., Pogorelko, V.V., Latypov, F.T., Ebel, A.A., 2020b. Interaction of dislocation with GP zones or theta ’’ phase precipitates in aluminum: atomistic simulations and dislocation dynamics. Int. J. Plast. 125, 169–190.
Lei, Z., Liu, X., Wu, Y., Wang, H., Jiang, S., Wang, S., Hui, X., Wu, Y., Gault, B., Kontis, P., Raabe, D., Gu, L., Zhang, Q., Chen, H., Wang, H., Liu, J., An, K., Zeng, Q., Nieh, T.G., Lu, Z., 2018. Enhanced strength and ductility in a high-entropy alloy via ordered oxygen complexes. Nature 563 (7732), 546–550.
Li, Z., Tasan, C.C., Springer, H., Gault, B., Raabe, D., 2017. Interstitial atoms enable joint twinning and transformation induced plasticity in strong and ductile high-entropy alloys. Sci. Rep. 7 (1), 40704.
Lu, K., Lu, L., Suresh, S., 2009. Strengthening materials by engineering coherent internal boundaries at the nanoscale. Science 324 (5925), 349–352.
Lu, K., 2010. The future of metals. Science 328 (5976), 319–320.
Ming, K., Bi, X., Wang, J., 2018. Realizing strength-ductility combination of coarse-grained Al0.2Co1.5CrFeNi1.5Ti0.3 alloy via nano-sized, coherent precipitates. Int. J. Plast. 100, 177–191.
Peng, S., Wei, Y., Jin, Z., Yang, W., 2019. Supersonic screw dislocations gliding at the shear wave speed. Phys. Rev. Lett. 122 (4), 045501.
Peng, S., Wei, Y., Gao, H., 2020. Nanoscale precipitates as sustainable dislocation sources for enhanced ductility and high strength. Proc. Natl. Acad. Sci. 117 (10), 5204–5209.
Plimpton, S., 1995. Fast parallel algorithms for short-range molecular dynamics. J. Comput. Phys. 117, 1–19.
Poole, W.J., Wang, X., Lloyd, D.J., Embury, J.D., 2005. The shearable–non-shearable transition in Al–Mg–Si–Cu precipitation hardening alloys: implications on the distribution of slip, work hardening and fracture. Philos. Mag. 85 (26–27), 3113–3135.
Proville, L., Bakó, B., 2010. Dislocation depinning from ordered nanophases in a model fcc crystal: from cutting mechanism to Orowan looping. Acta Mater. 58 (17), 5565–5571.
Raabe, D., Ponge, D., Dmitrieva, O., Sander, B., 2009. Nanoprecipitate-hardened 1.5GPa steels with unexpected high ductility. Scr. Mater. 60 (12), 1141–1144.
Ritchie, R.O., 2011. The conflicts between strength and toughness. Nat. Mater. 10 (11), 817–822.
Shao, C.W., Zhang, P., Zhu, Y.K., Zhang, Z.J., Tian, Y.Z., Zhang, Z.F., 2018. Simultaneous improvement of strength and plasticity: additional work-hardening from gradient microstructure. Acta Mater. 145, 413–428.
Shi, G., Chen, X., Jiang, H., Wang, Z., Tang, H., Fan, Y., 2015. Strengthening mechanisms of Fe nanoparticles for single crystal Cu–Fe alloy. Mater. Sci. Eng. A 636, 43–47.
Singh, C.V., Warner, D.H., 2010a. Mechanisms of Guinier–Preston zone hardening in the athermal limit. Acta Mater. 58 (17), 5797–5805.
Singh, C.V., Warner, D.H., 2010b. Mechanisms of Guinier-Preston zone hardening in the athermal limit. Acta Mater. 58 (17), 5797–5805.
Sjölander, E., Seifeddine, S., 2010. The heat treatment of Al–Si–Cu–Mg casting alloys. J. Mater. Process. Technol. 210 (10), 1249–1259.
Stukowski, A., 2010. Visualization and analysis of atomistic simulation data with OVITO–the Open Visualization Tool. Modell. Simul. Mater. Sci. Eng. 18 (1), 015012.
Sun, L., Simm, T.H., Martin, T.L., McAdam, S., Galvin, D.R., Perkins, K.M., Bagot, P.A.J., Moody, M.P., Ooi, S.W., Hill, P., Rawson, M.J., Bhadeshia, H.K.D.H., 2018. A novel ultra-high strength maraging steel with balanced ductility and creep resistance achieved by nanoscale β-NiAl and Laves phase precipitates. Acta Mater. 149, 285–301.
Sun, L.G., Wu, G., Wang, Q., Lu, J., 2020. Nanostructural metallic materials: structures and mechanical properties. Mater. Today 38, 114–135.
Szajewski, B.A., Crone, J.C., Knap, J., 2020. Analytic model for the Orowan dislocation-precipitate bypass mechanism. Materialia 11, 100671.

Tan, T.Y., Tice, W.K., 1976. Oxygen precipitation and the generation of dislocations in silicon. Philos. Mag. 34, 615–631.
Tsuzuki, H., Branicio, P.S., Rino, J.P., 2009. Molecular dynamics simulation of fast dislocations in copper. Acta Mater. 57 (6), 1843–1855.
Weertman, J., Keer, L.M., 1997. Dislocation based fracture mechanics. J. Appl. Mech. 64 (4), 1029. -1029.
Wu, B., Bai, Z., Misra, A., Fan, Y., 2020. Atomistic mechanism and probability determination of the cutting of Guinier-Preston zones by edge dislocations in dilute Al-Cu alloys. Phys. Rev. Mater. 4 (2), 020601.
Xiong, L.M., Xu, S.Z., McDowell, D.L., Chen, Y.P., 2015. Concurrent atomistic-continuum simulations of dislocation-void interactions in fcc crystals. Int. J. Plast. 65, 33–42.
Yang, T., Zhao, Y.L., Tong, Y., Jiao, Z.B., Wei, J., Cai, J.X., Han, X.D., Chen, D., Hu, A., Kai, J.J., Lu, K., Liu, Y., Liu, C.T., 2018. Multicomponent intermetallic nanoparticles and superb mechanical behaviors of complex alloys. Science 362 (6417), 933–937.
Yang, H., Li, K., Bu, Y., Wu, J., Fang, Y., Meng, L., Liu, J., Wang, H., 2021. Nanoprecipitates induced dislocation pinning and multiplication strategy for designing high strength, plasticity and conductivity Cu alloys. Scr. Mater. 195, 113741.